Stabilization of GTSE1 by cyclin D1-CDK4/6-mediated phosphorylation promotes cell proliferation: relevance in cancer prognosis

Nelson García-Vázquez[1], Tania J. González-Robles[1,2,3], Ethan Lane[1], Daria Spasskaya[1], Qingyue Zhang[1], Marc Kerzhnerman[1], YeonTae Jeong[1*], Marta Collu[1], Daniele Simoneschi[1], Kelly V. Ruggles[2], Gergely Rona[1,3,4], Sharon Kaisari[1,3], and Michele Pagano[1,3]

[1]Department of Biochemistry and Molecular Pharmacology, [2]Department of Medicine, and [3]Howard Hughes Medical Institute, New York University Grossman School of Medicine, NYC, NY, USA.
[4]Institute of Molecular Life Sciences, HUN-REN Research Centre for Natural Sciences, Budapest, Hungary.
[*]Current address: Arvinas Inc., New Haven, CT, USA.

Correspondence: michele.pagano@nyumc.org and sharon.kaisari@nyulangone.org

Key words: cyclin D1, CDK4, CDK6, cullin-RING ligases, cell proliferation

Abstract

In healthy cells, cyclin D1 is expressed during the G1 phase of the cell cycle, where it activates CDK4 and CDK6. Its dysregulation is a well-established oncogenic driver in numerous human cancers. The cancer-related function of cyclin D1 has been primarily studied by focusing on the phosphorylation of the retinoblastoma (RB) gene product. Here, using an integrative approach combining bioinformatic analyses and biochemical experiments, we show that GTSE1 (G-Two and S phases expressed protein 1), a protein positively regulating cell cycle progression, is a previously unrecognized substrate of cyclin D1-CDK4/6 in tumor cells overexpressing cyclin D1 during G1 and subsequent phases. The phosphorylation of GTSE1 mediated by cyclin D1-CDK4/6 inhibits GTSE1 degradation, leading to high levels of GTSE1 across all cell cycle phases. Functionally, the phosphorylation of GTSE1 promotes cellular proliferation and is associated with poor prognosis within a pan-cancer cohort. Our findings provide insights into cyclin D1's role in cell cycle control and oncogenesis beyond RB phosphorylation.

Introduction

D-type cyclins (cyclin D1, cyclin D2 and cyclin D3) are activators of the cyclin-dependent kinases CDK4 and CDK6 and represent major oncogenic drivers among members of the cyclin superfamily[1-4]. The *CCND1* gene --encoding cyclin D1-- shows some of the highest frequency of amplification and overexpression among cancer genes across a broad spectrum of human tumors[5-9]. Moreover, mutations in *CCND1*, which prevent the degradation of cyclin D1 by AMBRA1, a substrate receptor (SR) of a CUL4-RING ubiquitin ligase (CRL4) complex that targets all three D-type cyclins for proteasome-mediated degradation, have been reported in a variety of tumor types[10-12]. Deregulation of cellular proliferation, often mediated by uncontrolled CDKs' activation lies at the heart of cancer as a pathological process[13].

The biological roles of D-type cyclins have been examined almost exclusively through the lens of E2F transcription regulation upon phosphorylation of the three pocket proteins, RB, p107, and p130. D type cyclins-mediated phosphorylation of RB results in the inactivation of its tumor suppressive effect by releasing E2F from the RB's inhibitory effect on gene transcription. Although the regulation of RB by phosphorylation is well understood in both physiology and human tumorigenesis, the cancer-related role of phosphorylation of other substrates is a subject that has remained understudied. In this study, we characterize GTSE1 (G-Two and S-phase expressed protein 1) as a previously unidentified substrate of cyclin D1-CDK4/6 in cells overexpressing cyclin D1 in G1 and beyond. GTSE1 is a cell cycle-related protein expressed specifically during the S and G2 phases of the cell cycle[14]. It interacts with the tumor suppressor p53, and it induces its MDM2-mediated degradation in G2 and during the recovery from DNA damage, promoting cell proliferation[14-19]. Moreover, GTSE1 associates with growing microtubules, promoting cell

migration[20,21]. In prometaphase, GTSE1 becomes highly phosphorylated by CDK1-cyclin B1, resulting in its recruitment to the inner spindle[22]. After anaphase, its dephosphorylation is followed by marked reduction in its abundance in G1[18,23]. Our findings demonstrate that the cyclin D1-CDK4/6-mediated phosphorylation of GTSE1 leads to its increased stability in G1 phase, an event that significantly impacts cell proliferation and cancer prognosis.

Results and discussion

AMBRA1 is a substrate receptor of a CUL4-RING ubiquitin ligase (CRL4) complex that targets all three D-type cyclins for proteasome-mediated degradation[10,11]. To unveil new substrates of the cyclin D1-CDK4 complex, we performed a comprehensive muti-analysis of published data (Figure supplement 1A). First, we incorporated recent mass spectrometry data that compared the whole proteome of AMBRA1 knockout (KO) clones to parental U2OS cells[11], aiming to pinpoint the top 30 proteins whose levels were elevated in the absence of AMBRA1, the SR of the ubiquitin ligase targeting D-type cyclins (Figure 1A). Subsequently, we asked which of these 30 proteins contain a canonical CDK phosphorylation consensus motif [S/T*]PX[K/R], relying on the PhosphoSitePlus database[24] (Figure 1B). Finally, this dataset was integrated with findings from a proteomic screen assessing protein abundance fluctuations in the presence or absence of the CDK4/6 inhibitor, Palbociclib (Figure 1C)[11]. In summary, our analysis aimed at identifying proteins whose upregulation in AMBRA1 KO cells was counteracted by Palbociclib treatment, thereby filtering for proteins whose augmented abundance is attributed to CDK4/6-mediated phosphorylation events when cyclin D1 is stabilized. GTSE1, a cell cycle-regulated protein expressed mainly during the G2 and S phases of the cell cycle[14], emerged as the top hit in these orthogonal analyses. In mitosis

GTSE1 is phosphorylated by CDK1-cyclin B1[22], but its dephosphorylation at the end of mitosis is followed by marked reduction in its abundance, which remains low during the next G1[18,23].

Recent pan-cancer analysis revealed that the expression of GTSE1 positively correlates with tumor mutational burden and microsatellite instability in most cancer types[25]. Specifically, high expression of GTSE1 was found to promote the proliferation and invasion of breast cancer cells[26], and was associated with poor clinical prognosis in clear cell renal cell carcinoma[27]. We explored further the potential influence of GTSE1 on cancer prognosis and found that within multiple cancer cohorts, its elevated expression levels were correlated with a statistically significant poorer prognosis compared to lower expression levels (Figure 1D, Figure supplement 1B). This is noteworthy, since, except for acute myeloid leukemia (LAML), GTSE1 expression was higher than that in normal tissue counterparts in all tumor types analyzed (Figure 1E). We also assessed the impact of GTSE1 on survival across various cancer types (Figure 1F, Figure supplement 1B). For context, we compared the survival patterns associated with cyclin D1, CDK4, and CDK6. Similar to the overexpression of other cell cycle-regulated genes[28], high levels of GTSE1 were found to be prognostically unfavorable across multiple cancer types, presenting a survival pattern similar to that of the cyclin D1-CDK4/6 gene cluster. In Figure 1F, those cancers in which differences in survival are statistically significant were denoted by contour squares.

Next, we sought to experimentally validate GTSE1 as a putative phosphorylation target of cyclin D1-CDK4. As a first step, we employed transient transfection to introduce in HEK293T various Flag-tagged constructs in the presence or absence of cyclin D1 and CDK4. GTSE1 showed an upper shift in a phos-tag™ gel when co-expressed with cyclin D1-CDK4, similar to the known substrates p107

and p130 (Figure 2A). In fact, a slight delay in GTSE1 migration is appreciable even in a regular SDS-PAGE (see first two lanes in Figure 2A). The upper shift was not observed in ZC3HAV1, a protein used as negative control. Next, we performed an *in vitro* phosphorylation assay to directly assess the specificity of GTSE1 phosphorylation by cyclin D1-CDK4. Using purified, recombinant proteins, we subjected GTSE1 to a phosphorylation reaction with cyclin D1-CDK4 and analyzed the products using phos-tag™ gels. The results confirmed that GTSE1 underwent phosphorylation by cyclin D1-CDK4, but not by ERK1, another Pro-directed kinase (Figure 2B). Moreover, the phosphorylation was abolished in the presence of Palbociclib, similar to the pattern observed with RB (Figure 2B,C,H). Then, we asked whether GTSE1 physically interacts with the kinase complex. Overexpression of Flag-tagged cyclin D1 and CDK4 in HEK293T followed by a Flag pull-down demonstrated binding to endogenous GTSE1, similar to the canonical substrate RB (Figure 2D).

Following these validation steps, we aimed at pinpointing the serine residue(s) modified by cyclin D1-CDK4. First, we generated a GTSE1 mutant in which Ser262 (see Figure 1B) was mutated to Ala. Since GTSE1 has additional, conserved serine residues followed by prolines, which could be potential CDK phosphorylation sites (Figure 2E, Figure supplement 2A-B), we also generated another sixteen Ser-to-Ala GTSE1 mutants and expressed them in HEK293T cell in the presence or absence of cyclin D1-CDK4 (Figure supplement 3A). When compared to wild-type GTSE1, two mutants displayed changes in their migrations on phos-tag™ gels (Figure supplement 3A), suggesting that Ser residues at positions 91 and 724 are sites potentially phosphorylated by cyclin D1-CDK4. PhosphoSitePlus[24] reports several high-throughput studies that, in addition to Ser262, identified phosphorylation also at Ser91 and Ser724, supporting our results. To corroborate the loss of cyclin D1-CDK4-dependent phosphorylation at these sites, we constructed a triple mutant

(S91A/S262A/S724A). This triple mutant displayed loss of slower-migrating bands relative to wild-type GTSE1, suggesting diminished phosphorylation (Figure 2F). Nevertheless, a residual slow-migrating band persisted, prompting further mutations of the triple GTSE1 mutant in two additional GTSE1 sites (individually), which do not have a CDK-phosphorylation consensus, but were identified in several proteomics studies[24,29]. From these two mutants, only the S454A mutation demonstrated a complete abrogation of any shift in phos-tag™ gels (Figure 2F). In contrast, a single S454A mutation showed only a minor effect on GTSE1 shift (data not shown). These studies suggest that four major sites (S91, S262, S454, and S724) are phosphorylated (either directly and/or indirectly) in a cyclin D1-CDK4-dependent manner.

To gain an insight into the cell-cycle pattern of GTSE1 abundance and phosphorylation status, we synchronized T98G cells (both parental and AMBRA1 knockout [KO] pooled clones) by serum starvation followed by serum re-addition. Parental cells displayed a fluctuation in GTSE1 abundance, with low levels in G1 that subsequently increased in S and G2 phases (Figure supplement 3B), in agreement with the literature[18,23]. In contrast, in AMBRA1 KO cells, GTSE1 levels were consistently elevated throughout the cell cycle, suggesting that elevated cyclin D1 levels are associated with an increased abundance of GTSE1 (Figure supplement 3B). Additionally, while phosphorylation of GTSE1 in the parental cell line peaked during the G2/M transition (28-32 hours after serum readdition), AMBRA1 KO cells exhibited sustained phosphorylation of GTSE1 across all cell cycle phases (Figure 2G and Figure supplement 3B). We also generated a phospho-specific antibody that recognized GTSE1 only when phosphorylated on Ser262 (Figure supplement 3C). Using this antibody, we confirmed the data obtained with phos-tag™ gel indicating that in cells

overexpressing cyclin D1-CDK4 and in AMBRA1 KO cells, GTSE1 is hyper-phosphorylated on Ser262 (Figure 2G and Figure supplement 3C).

Next, we leveraged data from the Clinical Proteomic Tumor Analysis Consortium (CPTAC) to examine the relevance of the identified phosphorylation events in a clinical context. We observed an enrichment of GTSE1 phospho-peptides within a pan-cancer cohort as opposed to adjacent, corresponding normal tissues (Figure 2I), underscoring the potential role of GTSE1 phosphorylation in tumorigenesis. Upon analyzing single phosphorylated sites, we found that nine were statistically enriched in cancers. Of these, three sites (S262, S454, and S724) were identified as dependent on cyclin D1-CDK4 in our study (Figure 2J and Figure supplement 3D). (Data on Ser91 are not present in CPTAC.) These results underscore the potential pathophysiological significance of GTSE1 phosphorylation by cyclin D1-CDK4 in cancer.

Considering GTSE1 being an established target of cyclin B1-CDK1 during mitosis[22], we aimed to elucidate the phosphorylation patterns of GTSE1 by various cyclin-CDK complexes operating at distinct cell cycle phases. Wild-type GTSE1 was found to be phosphorylated in HEK293T cells upon overexpression of all cyclin-CDK pairs, with its shifts in phos-tag™ gels being abolished upon treatment with the corresponding specific CDK inhibitor (Figure 2H, left panel). However, when the quadruple (S91A/S262A/S454A/S724A) GTSE1 mutant, referred to as “Tetra SA”, was expressed in HEK293T cells, cyclin D1-CDK4 was unable to induce any shift, whereas the other three cyclin-CDK pairs still sustained phosphorylation (Figure 2H, right panel). This suggests a unique phosphorylation profile conferred by cyclin D1-CDK4 in GTSE1, distinct from that induced by other cyclin-CDK complexes.

We noticed an elevation in endogenous GTSE1 levels in AMBRA1 knockout cells compared to the parental line (Figure supplement 3B and Figure 3A) in agreement with the findings of the proteomic screen performed in AMBRA1 KO cells[11] (Figure 1B). A similar increase was observed when overexpressing wild-type cyclin D1 and, even more, an AMBRA1-insensitive, stable mutant of cyclin D1 (T286A)[10] (Figure 3A,B), suggesting that the elevated GTSE1 levels are due to high D-type cyclins present in AMBRA1 knockout cells. We also used HCT116 cells harboring an endogenous fusion of AMBRA1 to a minimally constructed Auxin Inducible Degron (mAID) at the N-terminus[30]. This system allows for rapid and inducible degradation of AMBRA1 upon addition of auxin, thereby minimizing compensatory cellular rewiring. Again, we observed an increase in GTSE1 levels upon acute ablation of AMBRA1 (*i.e.,* in 8 hours) (Figure 3B). In all cases, the upregulation in GTSE1 abundance was rescued upon Palbociclib treatment (Figure 3A,B), suggesting that this event was a consequence of increased levels of D-type cyclins. We also conducted cycloheximide chase assays in HCT-116 mAID-AMBRA1 cells to assess GTSE1 protein stability and degradation kinetics. The assays revealed that in the context of AMBRA1 depletion, GTSE1 exhibited a prolonged half-life and reduced degradation rate when compared to control cells (Figure 3C). A parallel half-life assessment in parental U2OS cells and two AMBRA1 knockout U2OS clones corroborated the finding that GTSE1 is stabilized in the absence of AMBRA1 (Figure 3D).

To further dissect the impact of cyclin D1-CDK4-mediated phosphorylation on GTSE1 stability, we engineered a phospho-mimicking mutant, referred to as “Tetra SD” with the 4 serine residues replaced with an aspartate at positions 91, 261, 454, and 724. To circumvent the variability of transient transfection, U2OS cells were stably transduced with retroviruses encoding GFP-tagged

206 wild-type GTSE1, Tetra SA (phospho-deficient), or Tetra SD (phospho-mimic). Subsequent CHX
207 chase experiments showed a slower degradation kinetics of the Tetra SD mutant compared to the
208 Tetra SA mutant and wild-type GTSE1 (Figure 3E,F). These stable cell lines, expressing fluorescent
209 GTSE1 variants, were further analyzed via time-lapse microscopy during a CHX chase to quantify
210 protein degradation through the diminishing fluorescence intensity at different times. The Tetra SD
211 mutant exhibited a statistically significant slower fluorescence decrease rate than both Tetra SA and
212 WT, indicating reduced degradation (Figure 3G,H).
213
214 Finally, we treated U2OS cells with CHX together with inhibitors targeting different degradation
215 systems: MG132 (a proteasome inhibitor), MLN4924 (a CRL inhibitor), or Bafilomycin A (an
216 autophagy inhibitor) (Figure 3I). The stabilization of GTSE1 in the presence of MG132 and
217 MLN4924, but not Bafilomycin A, indicates that GTSE1 degradation mainly occurs via the ubiquitin-
218 proteasome system (UPS), specifically implicating the involvement of a CRL. However, GTSE1 does
219 not appear to be a substrate of $CRL4^{AMBRA1}$, as indicated by the lack of a physical interaction
220 between AMBRA1 and GTSE1 (Figure supplement 3E), as well as the fact that the stabilization of
221 GTSE1 in AMBRA1 KO cells is secondary to the CDK4/6 activity (Figure 3A,B).
222
223 Next, we delved into the potential implications of GTSE1 phosphorylation by the cyclin D1-CDK4
224 complex. Previous research has connected GTSE1 with fundamental cellular processes, such as cell
225 proliferation[27,31] and cell migration and invasion[21,32,33]. Leveraging data from CPTAC, we examined
226 possible correlations between both GTSE1 protein levels (Figure supplement 4A) and levels of
227 phosphorylated GTSE1 (Figure 4A) with markers of cell proliferation and cell migration across
228 various cancer types. GTSE1 abundance and phosphorylation exhibited a statistically significant

229 positive correlation with several proteins integral to cell proliferation, including PCNA, KI67, and
230 MCM2, across multiple cancer cohorts. Conversely, in contrast to data suggesting a role for GTSE1 in
231 promoting cell migration[21,26,27,32], GTSE1 levels and phosphorylation demonstrated a negative trend
232 with proteins associated with cell migration and epithelial-mesenchymal transition (EMT), such as
233 Vimentin, MMP1, and ETS1, but these did not attain statistical significance.
234
235 To explore the influence of cyclin D1-mediated phosphorylation of GTSE1 on cellular phenotypes,
236 we assessed the proliferation potential of AMBRA1 knockout cells relative to their parental
237 counterparts. AMBRA1 KO cells displayed an enhanced proliferation rate (Figure supplement 4B),
238 in agreement with the literature[10]. We then conducted comparable growth analyses using U2OS
239 cells stably expressing various GTSE1 constructs. Cells stably expressing the Tetra SD mutant
240 exhibited a higher proliferation rate compared to cells expressing either Tetra SA or WT GTSE1
241 (Figure 4B). Moreover, evaluations of cellular proliferation conducted using Cell Trace dye
242 demonstrated that cells harboring the Tetra-SD mutant displayed an elevated proliferative index
243 (Figure 4C and Figure supplement 4D-E). This was evidenced by a greater number of cell
244 generations and smaller fraction of non-divided cells relative to cells expressing WT GTSE1 and,
245 even more so compared to cells expressing Tetra SA (Figure 4C and Figure supplement 4D-E).
246 Finally, cell cycle profiles showed that the expression of a phospho-mimicking GTSE1 mutant
247 induces a decrease in the percentage of cells in G1 and an increase in the percentage of cells in S,
248 similarly to what observed in AMBRA1 KO cells (Figure supplement 4F and Ref. [34]).
249
250 Cyclin D1 overexpression is a hallmark of many cancers, where it facilitates oncogenic
251 transformation and progression. Amplifications and overexpression of the *CCND1* gene are seen in a

diverse array of cancers, with amplifications in up to 15% to 20% of breast cancers and overexpression in over 50% of mantle cell lymphomas[1,35]. The pervasiveness of cyclin D1 dysregulation in cancer highlights the critical need to understand its downstream effects. Despite this, the full spectrum of substrates and their impact on cellular function and oncogenesis has yet to be thoroughly investigated[29,36-39]. In the present study, we identified GTSE1, a pro-proliferative protein, as a novel substrate of the cyclin D1-CDK4 complex in tumor cells overexpressing cyclin D1 during G1 and subsequent phases. Our data indicate that cyclin D1-CDK4 is responsible for the phosphorylation of GTSE1 on four residues (S91, S262, S454, and S724). In contrast, cyclin A2-CDK2, cyclin E1-CDK2, and cyclin B1-CDK1 target additional and/or different sites as shown by the fact that they still induced mobility shift of the "Tetra SA" mutant in cultured cells. GTSE1 has been established as a substrate of mitotic cyclins[14,22,23], but we observed that in human cells, when D-type cyclins are stabilized in the absence of AMBRA1, GTSE1 becomes phosphorylated across the various cell cycle phases. Accordingly, overexpression of cyclin D1-CDK4 induce GTSE1 phosphorylation. Thus, we propose that GTSE1 is phosphorylated by CDK4 and CDK6 particularly in pathological states, such as cancers displaying overexpression of D-type cyclins. In turn, GTSE1 phosphorylation induces its stabilization, leading to increased levels that contribute to enhanced cell proliferation. It is also possible that GTSE1 is also recognized in specific cell types and in particular stage/s of embryogenesis, when cyclin D1 levels are elevated, and high cell proliferation is crucial for proper tissue formation[40]. The prolonged half-life of GTSE1 consequent to cyclin D1-CDK4-mediated phosphorylation suggests a mechanism through which cells could modulate the abundance of a key regulatory protein without necessitating new protein synthesis. This post-translational regulation could be a critical determinant in the rapid response to mitogenic signals or environmental cues.

Our study further established a correlation between phosphorylation of GTSE1 and markers of cell proliferation, as well as poor prognosis in human cancers, providing a partial explanatory basis for the proliferative phenotype associated with elevated D-type cyclins observed in human tumors. Future studies are warranted to further dissect the molecular mechanisms underpinning GTSE1's contribution to the cancerous phenotype, potentially paving the way for novel cancer therapeutics.

REFERENCES

1 Musgrove, E. A., Caldon, C. E., Barraclough, J., Stone, A. & Sutherland, R. L. Cyclin D as a therapeutic target in cancer. *Nat Rev Cancer* **11**, 558-572 (2011). https://doi.org:10.1038/nrc3090

2 Fassl, A., Geng, Y. & Sicinski, P. CDK4 and CDK6 kinases: From basic science to cancer therapy. *Science* **375**, eabc1495 (2022). https://doi.org:10.1126/science.abc1495

3 Alvarez-Fernandez, M. & Malumbres, M. Mechanisms of Sensitivity and Resistance to CDK4/6 Inhibition. *Cancer Cell* **37**, 514-529 (2020). https://doi.org:10.1016/j.ccell.2020.03.010

4 Behan, F. M. *et al.* Prioritization of cancer therapeutic targets using CRISPR-Cas9 screens. *Nature* **568**, 511-516 (2019). https://doi.org:10.1038/s41586-019-1103-9

5 Beroukhim, R. *et al.* The landscape of somatic copy-number alteration across human cancers. *Nature* **463**, 899-905 (2010). https://doi.org:10.1038/nature08822

6 Curtin, J. A. *et al.* Distinct sets of genetic alterations in melanoma. *N Engl J Med* **353**, 2135-2147 (2005). https://doi.org:10.1056/NEJMoa050092

7 Bignell, G. R. *et al.* Signatures of mutation and selection in the cancer genome. *Nature* **463**, 893-898 (2010). https://doi.org:10.1038/nature08768

8 Parsons, D. W. *et al.* An integrated genomic analysis of human glioblastoma multiforme. *Science* **321**, 1807-1812 (2008). https://doi.org:10.1126/science.1164382

9 Jones, S. *et al.* Core signaling pathways in human pancreatic cancers revealed by global genomic analyses. *Science* **321**, 1801-1806 (2008). https://doi.org:10.1126/science.1164368

10 Simoneschi, D. *et al.* CRL4(AMBRA1) is a master regulator of D-type cyclins. *Nature* (2021). https://doi.org:10.1038/s41586-021-03445-y

11 Chaikovsky, A. C. *et al.* The AMBRA1 E3 ligase adaptor regulates the stability of cyclin D. *Nature* **592**, 794-798 (2021). https://doi.org:10.1038/s41586-021-03474-7

12 Martinez-Jimenez, F. *et al.* A compendium of mutational cancer driver genes. *Nat Rev Cancer* **20**, 555-572 (2020). https://doi.org:10.1038/s41568-020-0290-x

13 Kastan, M. B. & Bartek, J. Cell-cycle checkpoints and cancer. *Nature* **432**, 316-323 (2004). https://doi.org:10.1038/nature03097

14 Liu, X. S., Li, H., Song, B. & Liu, X. Polo-like kinase 1 phosphorylation of G2 and S-phase-expressed 1 protein is essential for p53 inactivation during G2 checkpoint recovery. *EMBO Rep* **11**, 626-632 (2010). https://doi.org:10.1038/embor.2010.90

15 Bublik, D. R., Scolz, M., Triolo, G., Monte, M. & Schneider, C. Human GTSE-1 regulates p21(CIP1/WAF1) stability conferring resistance to paclitaxel treatment. *J Biol Chem* **285**, 5274-5281 (2010). https://doi.org:10.1074/jbc.M109.045948

16 Monte, M. *et al.* The cell cycle-regulated protein human GTSE-1 controls DNA damage-induced apoptosis by affecting p53 function. *J Biol Chem* **278**, 30356-30364 (2003). https://doi.org:10.1074/jbc.M302902200

17 Monte, M. *et al.* hGTSE-1 expression stimulates cytoplasmic localization of p53. *J Biol Chem* **279**, 11744-11752 (2004). https://doi.org:10.1074/jbc.M311123200

18 Collavin, L., Monte, M., Verardo, R., Pfleger, C. & Schneider, C. Cell-cycle regulation of the p53-inducible gene B99. *FEBS Lett* **481**, 57-62 (2000). https://doi.org:10.1016/s0014-5793(00)01969-4

19 Utrera, R., Collavin, L., Lazarevic, D., Delia, D. & Schneider, C. A novel p53-inducible gene coding for a microtubule-localized protein with G2-phase-specific expression. *EMBO J* **17**, 5015-5025 (1998). https://doi.org:10.1093/emboj/17.17.5015

20 Bendre, S. *et al.* GTSE1 tunes microtubule stability for chromosome alignment and segregation by inhibiting the microtubule depolymerase MCAK. *J Cell Biol* **215**, 631-647 (2016). https://doi.org:10.1083/jcb.201606081

21 Scolz, M. *et al.* GTSE1 is a microtubule plus-end tracking protein that regulates EB1-dependent cell migration. *PLoS One* **7**, e51259 (2012). https://doi.org:10.1371/journal.pone.0051259

22 Singh, D., Schmidt, N., Muller, F., Bange, T. & Bird, A. W. Destabilization of Long Astral Microtubules via Cdk1-Dependent Removal of GTSE1 from Their Plus Ends Facilitates Prometaphase Spindle Orientation. *Curr Biol* **31**, 766-781 e768 (2021). https://doi.org:10.1016/j.cub.2020.11.040

23 Monte, M. *et al.* Cloning, chromosome mapping and functional characterization of a human homologue of murine gtse-1 (B99) gene. *Gene* **254**, 229-236 (2000). https://doi.org:10.1016/s0378-1119(00)00260-2

24 Hornbeck, P. V. *et al.* PhosphoSitePlus, 2014: mutations, PTMs and recalibrations. *Nucleic Acids Res* **43**, D512-520 (2015). https://doi.org:10.1093/nar/gku1267

25 Tan, K. *et al.* Pan-cancer analyses reveal GTSE1 as a biomarker for the immunosuppressive tumor microenvironment. *Medicine (Baltimore)* **102**, e34996 (2023). https://doi.org:10.1097/MD.0000000000034996

26 Lin, F. *et al.* GTSE1 is involved in breast cancer progression in p53 mutation-dependent manner. *J Exp Clin Cancer Res* **38**, 152 (2019). https://doi.org:10.1186/s13046-019-1157-4

27 Lei, P., Zhang, M., Li, Y. & Wang, Z. High GTSE1 expression promotes cell proliferation, metastasis and cisplatin resistance in ccRCC and is associated with immune infiltrates and poor prognosis. *Front Genet* **14**, 996362 (2023). https://doi.org:10.3389/fgene.2023.996362

28 Whitfield, M. L., George, L. K., Grant, G. D. & Perou, C. M. Common markers of proliferation. *Nat Rev Cancer* **6**, 99-106 (2006). https://doi.org:10.1038/nrc1802

29 Kaulich, M. *et al.* A Cdk4/6-dependent phosphorylation gradient regulates the early to late G1 phase transition. *Sci Rep* **11**, 14736 (2021). https://doi.org:10.1038/s41598-021-94200-w

30 Yesbolatova, A. *et al.* The auxin-inducible degron 2 technology provides sharp degradation control in yeast, mammalian cells, and mice. *Nat Commun* **11**, 5701 (2020). https://doi.org:10.1038/s41467-020-19532-z

31 Lai, W. *et al.* GTSE1 promotes prostate cancer cell proliferation via the SP1/FOXM1 signaling pathway. *Lab Invest* **101**, 554-563 (2021). https://doi.org:10.1038/s41374-020-00510-4

32 Wu, X. *et al.* GTSE1 promotes cell migration and invasion by regulating EMT in hepatocellular carcinoma and is associated with poor prognosis. *Sci Rep* **7**, 5129 (2017). https://doi.org:10.1038/s41598-017-05311-2

33 Li, S. S. *et al.* GTSE1 promotes SNAIL1 degradation by facilitating its nuclear export in hepatocellular carcin oma cells. *Mol Med Rep* **23** (2021). https://doi.org:10.3892/mmr.2021.12093

34 Rona, G. *et al.* CDK-independent role of D-type cyclins in regulating DNA mismatch repair. *Mol Cell* **84**, 1224-1242 e1213 (2024). https://doi.org:10.1016/j.molcel.2024.02.010

35 Cancer Genome Atlas Research, N. Comprehensive genomic characterization of squamous cell lung cancers. *Nature* **489**, 519-525 (2012). https://doi.org:10.1038/nature11404

36 Sherr, C. J. Cell cycle control and cancer. *Harvey Lect* **96**, 73-92 (2000).

37 Knudsen, E. S. & Knudsen, K. E. Tailoring to RB: tumour suppressor status and therapeutic response. *Nat Rev Cancer* **8**, 714-724 (2008). https://doi.org:10.1038/nrc2401

38 Topacio, B. R. *et al.* Cyclin D-Cdk4,6 Drives Cell-Cycle Progression via the Retinoblastoma Protein's C-Terminal Helix. *Mol Cell* **74**, 758-770 e754 (2019). https://doi.org:10.1016/j.molcel.2019.03.020

39 Tchakarska, G. & Sola, B. The double dealing of cyclin D1. *Cell Cycle* **19**, 163-178 (2020). https://doi.org:10.1080/15384101.2019.1706903

40 Ter Huurne, M. & Stunnenberg, H. G. G1-phase progression in pluripotent stem cells. *Cell Mol Life Sci* **78**, 4507-4519 (2021). https://doi.org:10.1007/s00018-021-03797-8

41 Ellis, M. J. *et al.* Connecting genomic alterations to cancer biology with proteomics: the NCI Clinical Proteomic Tumor Analysis Consortium. *Cancer Discov* **3**, 1108-1112 (2013). https://doi.org:10.1158/2159-8290.CD-13-0219

42 Tang, Z., Kang, B., Li, C., Chen, T. & Zhang, Z. GEPIA2: an enhanced web server for large-scale expression profiling and interactive analysis. *Nucleic Acids Res* **47**, W556-W560 (2019). https://doi.org:10.1093/nar/gkz430

43 Cancer Genome Atlas Research, N. *et al.* The Cancer Genome Atlas Pan-Cancer analysis project. *Nat Genet* **45**, 1113-1120 (2013). https://doi.org:10.1038/ng.2764

44 Varadarajan, A. R. *et al.* A Proteogenomic Resource Enabling Integrated Analysis of Listeria Genotype-Proteotype-Phenotype Relationships. *J Proteome Res* **19**, 1647-1662 (2020). https://doi.org:10.1021/acs.jproteome.9b00842

Materials and Methods

Cell Culture and Transduction

HEK293T, HCT116, T98G and U2OS cell lines were cultured under specific conditions suited to each cell type. HEK293T and T98G cells were cultured in DMEM (Dulbecco's Modified Eagle Medium), while HCT116 and U2OS cells were maintained in McCoy's 5A medium. All media were supplemented with 10% fetal bovine serum (FBS) and 1% penicillin-streptomycin and cells were incubated at 37°C in a humidified atmosphere containing 5% CO2.

For retroviral production, HEK293T cells were co-transfected with GTSE1 expression constructs along with VSVG and PAX packaging plasmids using Lipofectamine 3000 (Invitrogen) according to the manufacturer's instructions. Virus-containing supernatants were harvested 48 hours post-transfection, filtered through a 0.45 µm pore size filter, and used for transducing target HCT116 and U2OS cells in the presence of 8 µg/ml Polybrene. Stably transduced cells were selected by sorting for EGFP positive cells by cell sorter.

For transient transfection studies, HEK293T cells were transfected with various plasmids using PEI (Polysciences); HCT-116 and U-2 OS where transiently transfected with Lipofectamine 3000 (Thermo Fisher Scientific). Where indicated, 24 h after transfection, cells were treated with MG132 or MLN4924 for 4 h before collection, following a protocol optimized for maximal transfection efficiency and minimal cellular toxicity. Post-transfection, cells were maintained under standard culture conditions before being harvested for subsequent experiments.

Plasmids

Homo sapiens cDNAs were amplified by PCR using KAPA HiFi DNA Polymerase (Kapa Biosystems) and sub-cloned into a variety of vector backbones, including modified pCDNA3.1 vectors containing N-terminal Flag or HA and pBABE-PURO retroviral vectors containing N-terminal eGFP. FFSS indicates a tandem 2×Flag–2×Strep tag. Site-directed mutagenesis was performed using KAPA HiFi DNA Polymerase (Kapa Biosystems).

Western Blotting and antibodies

Protein extracts were prepared using RIPA buffer supplemented with protease inhibitors (Complete ULTRA, Roche) and phosphatase inhibitors (PhosSTOP, Roche). The insoluble fraction was removed by centrifugation (20,000g) for 15 min at 4 °C. Protein concentrations in cell lysates were normalized using the Pierce BCA Protein Assay Kit (Thermo Fisher Scientific), according to the manufacturer’s instructions. Proteins were separated by SDS-PAGE and transferred to PVDF membranes. Membranes were blocked with 5% non-fat dry milk and incubated with primary antibodies overnight at 4°C, followed by HRP-conjugated secondary antibodies. Enhanced chemiluminescence (ECL, Thermo Fisher Scientific) was used for detection.

For high-resolution separation of phosphorylated proteins, we used Phos-tag gels with 7.5% acrylamide and 40 µM Zn^{2+} (Fujifilm Wako Chemicals U.S.A.), except for the experiment in Figure 2G in which we used 6% acrylamide and 100 µM Zn^{2+}. Electrophoresis was performed at 50 volts, according to the manufacturer's instructions. The following antibodies were used: GTSE1 (1:1000, Bethyl Laboratories #A302-274A), β-actin (1:5,000, Sigma-Aldrich A5441), AMBRA1 (1:1,000, Proteintech Group 13762–1-AP), cyclin A (1:5,000, M.P. laboratory), cyclin B1 (1:5,000, M.P. laboratory), cyclin D1 (1:1,000, Abcam ab16663), p-cyclin D1 (T286) (1:1,000, Cell Signaling Technology 3300S), cyclin E (1:1,000, Santa Cruz Biotechnology sc-247), Flag (1:2,000, Sigma-Aldrich F1804), Flag (1:2,000, Sigma-Aldrich F7425), GST (1:5,000, GE Healthcare 27457701), HA

434 (1:2,000, Bethyl Laboratories A190–108A), LC-3 (1:5,000, Novus Biological NB100–2220), p21
435 (1:1,000, Cell Signaling Technology 2947S), p27 (1:1,000, BD Biosciences 610241), p62 (1:5,000,
436 MBL International PM045), RB (1:1,000, Cell Signaling Technology 9313S), RB (1:1,000, Cell
437 Signaling Technology 9309S), p-RB (S807/811) (1:1,000, Cell Signaling Technology 9308S), SKP1
438 (1:5,000, M.P. laboratory), α-tubulin (1:5,000, Sigma-Aldrich T6074). A phospho-specific antibody
439 against GTSE1 phosphorylated on Ser262 was generated by YenZym. Briefly, a peptide containing
440 the phospho-epitope, which includes amino acids 254-269 (KPKKEIPApSPSRTKIP) was
441 synthesized. This peptide was then used to immunize rabbits, using Cys-KLH as immunogen,
442 prompting the production of antibodies against the phospho-epitope. Following immunization,
443 phospho-specific antibodies were purified by utilizing a phosphorylated peptide conjugated affinity
444 matrix. To ensure the specificity and efficacy of the antibody, an ELISA was performed on both pre-
445 and post-purified serum.
446
447 **In vitro phosphorylation**
448 Assays were carried out using 1 microgram of recombinant substrate proteins in the presence or
449 absence of 0.1 microgram of kinase enzymes. Where indicated, 1 μM Palbociclib was added to
450 reaction mixtures containing CDK4 and Cyclin D1 and subjected to pre-incubation on ice for 10
451 minutes before the addition of the recombinant substrates. The phosphorylation reaction was
452 conducted in kinase reaction buffer, containing 25 mM Tris-HCl (pH 7.5), 5 mM beta-
453 glycerophosphate, 2 mM dithiothreitol (DTT), 0.1 mM Na3VO4, 10 mM MgCl2, and 2 mM ATP. The
454 reaction mixture was maintained at 30°C for a duration of 1 hour. To terminate the reaction,
455 Laemmli buffer containing SDS and beta-mercaptoethanol was added to the samples, followed by
456 heating at 95°C for 10 minutes.
457
458 **Chemicals and Reagents**
459 Cycloheximide, Bafilomycin A1, MG132, and MLN4924 were obtained from Sigma-Aldrich (United
460 States). PF-06873600 and Palbociclib were purchased from Selleckchem (United States).
461 RO-3306 was acquired from Roche (United States). Auxin (Indole-3-acetic acid) and Doxycycline
462 were sourced from Thermo Fisher Scientific (United States). Rb (Retinoblastoma Human
463 Recombinant) fused with a 6X His tag, containing the C-terminal 792-928 aa, was obtained from
464 Raybiotech (United States). GTSE1, full-length, with N-terminal GST and C-terminal HIS tag, was
465 sourced from Origene (United States). GST-tagged ERK2 was acquired from Abcam (United States).
466 His-tagged Human Cyclin D1 and CDK4 were obtained from LSBio (United States).
467
468 **Growth Curve Analysis**
469 Cell proliferation was assessed by plating cells at a fixed density and counting at specific intervals
470 using Vi-CELL BLU Cell Viability Analyzer (Beckman Coulter). For cell count normalization, Trypan
471 Blue exclusion was used to assess cell viability.
472
473 **Cell Proliferation Analysis**
474 Cells were labeled with the CellTrace™ Far Red dye (Invitrogen) according to the manufacturer's
475 instructions, ensuring that the initial fluorescence intensity was homogenous across the cell
476 population. This method relies on the principle of dye dilution to trace multiple generations of cells
477 through flow cytometry. Following labeling, the cells were cultured under appropriate conditions to
478 allow for cell division (confluency<70%). Following five generation time, samples were collected

and subjected to flow cytometric analysis. The progressive halving of the fluorescent dye intensity, as a result of cell division, was monitored, enabling the quantification of cell generations.

Cell Cycle Studies

T98G cells were synchronized by serum starvation. Subconfluent plates of cells were trypsinized washed with PBS, and replated in DMEM containing 0.01% FBS. Cells were kept in this medium for 72 hours before they were trypsinized and replated at 70% confluency in DMEM containing 10% FBS to allow for cell cycle re-entry. Cells were collected at various time points following serum re-addition by scraping. Cell cycle was also monitored through EdU and PI (propidium iodide) staining and FACS analysis following the instructions of the manufacture.

Time Lapse Fluorescence Monitoring:

For the monitoring of GFP-tagged GTSE1 degradation, U2OS cells were plated at a density of 50,000 cells per well within 96-well plates. Following a period of 24 hours from plating, the cells were subjected to live cell imaging using the Cytation 5 Cell Imaging Reader (BioTek, Winooski, VT), which is equipped with a dedicated module for real-time cell analysis. The imaging apparatus maintained the cells in an optimal environment, regulated at 37°C with 5% CO2 levels. A Far Red cell tracer dye was applied to the cells prior to imaging, providing a distinct cellular outline for accurate identification during subsequent analysis. Images were captured at predetermined intervals following treatment with cycloheximide (CHX). Fluorescent emissions from both EGFP and Far Red spectra were monitored. Post-acquisition, images were analyzed to measure the cumulative EGFP fluorescent intensity within the confines delineated by the Far Red cellular demarcation. All procedures were conducted in triplicates.

Bioinformatic Analysis:

Bioinformatic analysis was performed using R statistical packages. For the visualization of tables, the 'formattable' package in R was employed. Differential proteomic profiling comparing parental U2OS cells to AMBRA1 knockout (KO) U2OS cells, utilized raw data from a shotgun proteomic screen previously published[11]. Proteins differentially expressed with an adjusted p-value < 0.05 were ordered according to the log2 fold change (Log2FC) comparing AMBRA1 KO to parental cells. The significance of the differentially expressed proteins was determined by the False Discovery Rate (FDR) method. An annotated list of phosphorylated proteins that contain the canonical CDK phosphorylation site [S/T*]PX[K/R] utilized the PhosphoSitePlus database[24]. This list was integrated with the proteomic data from the prior screen by matching gene names, to identify potential CDK substrates altered in the AMBRA1 KO context. The bioinformatic analysis for assessing the differential abundance and phosphorylation levels of GTSE1, as well as the correlation of GTSE1 abundance with different protein signatures in various cancer cohorts was conducted utilizing data from the Clinical Proteomic Tumor Analysis Consortium (CPTAC) database[41].

Acknowledgement

We thank Dr. Gregory David for critically reading the manuscript. MP is thankful to TM Thor and TB Balduur for their continuous support. This work was supported by NIH GM136250 to MP. MP is an investigator with the Howard Hughes Medical Institute. SK is a recipient of the Life Sciences Research Foundation (LSRF) Postdoctoral Fellowship and has been an EMBO Long Term Postdoctoral Fellow. NGV and TJGR are thankful for NIH Institutional Training Grant (T32GM136542). TJGR and KVR thank HHMI for Gilliam Fellowship (GT15758) support.

Author contributions

MP conceived, supervised, and coordinated the study. SK supervised and coordinated the study. NGV, DS, GR, and SK designed, carried out the experiments, and analyzed the data. For some experiments, they were helped by EL, MK, D Spasskaia and QZ. TJGR and KVR performed the CPTAC related analyses. SK and MP wrote the paper with input from all authors.

Declaration of interests

MP is or has been an advisor for and has financial interests in SEED Therapeutics, Triana Biomedicines, and CullGen, Kymera Therapeutics, Serinus Biosciences, and Umbra Therapeutics. The other authors have no competing interests to declare.

Figure legends

Figure 1: Identification of GTSE1 as a cyclin D1-CDK4 substrate with prognostic significance in cancer

A) Differential proteomic profiling of AMBRA1 KO U2OS cells compared to parental U2OS cells[11]. Proteins with adjusted p value<0.05 were ranked by the log2 fold change (Log2FC) to quantify expression changes between AMBRA1 KO and parental cells. The top 30 upregulated proteins in this analysis are presented. Statistical significance was assessed by False Discovery Rate (FDR).

B) Subset of proteins from (A) containing a canonical CDK phosphorylation consensus motif [S/T*]PX[K/R]. Annotated list of phosphorylated proteins was generated using PhosphoSitePlus database[24].

C) Subset of proteins from (B) whose abundance was reverted to basal levels following treatment of AMBRA1 KO U2OS cells with Palbociclib[11] (Log2FC_ambra) with adjusted p-values (adjp_ambra)<0.001 were ranked by log2 fold change (Log2FC) from the original shotgun proteomic analysis (A) to integrate expression changes between AMBRA1 KO and parental cells under Palbociclib-treated versus untreated condition.

D) Kaplan-Meier curves representing the overall survival analysis based on the 50% upper versus lower expression levels of GTSE1. Survival analysis was conducted across various cancer cohorts, including ACC, KIRP, KIRC, LGG, LUAD, MESO, PAAD, and SKCM (see also Figure supplement 1). The hazard ratio (HR) was calculated to estimate the relative risk, and significance was assessed using the log-rank test with a threshold of p<0.05. Curves were generated using the GEPIA2 platform.[42].

E) Transcriptomic analysis of GTSE1 in various cancer types, contrasting tumor (red) and normal tissue (blue) expression levels, using data derived from The Cancer Genome Atlas (TCGA)[43]. Statistical significance assessed by FDR, p<0.05.

F) Survival map of various cancer types according to the indicated gene expression levels (50% upper and lower expression). Color intensity indicates the log of the HR, with red and blue representing poorer and better survival, respectively. Statistically significant differences in survival are denoted by highlighted contour squares, based on the log-rank test. Generated with GEPIA2 platform[42], using TCGA data.

Figure 2: Cyclin D1-CDK4 promotes GTSE1 phosphorylation on four serine residues.

A) Immunoblot analysis following transient transfection of the indicated proteins in HEK293T cells detailing their phosphorylation status via differential mobility in phos-tag™ gels in the presence or absence of Cyclin D1-CDK4 co-expression.

B-C) The indicated purified, recombinant proteins were incubated in the presence or absence of recombinant cyclin D1-CDK4 complex. ERK2 was used as a negative control. Post-incubation, differential phosphorylation was analyzed using phos-tag™ gels to detect mobility shifts. Immunoblot analysis was conducted to verify the presence of the recombinant proteins as indicated.

D) HEK293T cells transfected with either the indicated Flag-tagged proteins or an empty vector (EV). Cell lysates were subjected to immunoprecipitation followed by immunoblot analysis. Inputs (5%) represent whole cell extracts before pull down.

E) Schematic representation of candidate CDK phosphorylation sites in GTSE1, as indicated by the PhosphoSitePlus database[24].

F) HEK293T cells were transiently transfected with the indicated HA-GTSE1 mutants, in the presence or absence of Cyclin D1-CDK4 co-expression. Changes in protein migration were analyzed by phos-tag™ gels.

G) Immunoblot and phos-tag™ gel analysis displaying cell cycle synchronization effects following 72 hours of serum starvation in parental T98G cells and AMBRA1 KO T98G cells. Cells were collected at various time points post-serum re-supplementation as indicated, followed by immunoblotting with the indicated antibodies.

H) HA-tagged wild type GTSE1 (left) or GTSE1 mutated at positions 91, 261, 454, and 724 ('Tetra SA') (right) was subjected to co-expression with various cyclins and CDKs, in the presence or absence of the indicated kinase inhibitors to observe the impact on phosphorylation.

I) Boxplot showing GTSE1 phosphorylation levels normalized to total GTSE1 protein abundance across a pan-cancer cohort relative to adjacent normal tissue, utilizing data from the Clinical Proteomic Tumor Analysis Consortium (CPTAC)[44]. Statistical significance was assessed using the Wilcoxon rank-sum test, with a p-value threshold of <0.05.

J) Heatmap illustrating differential abundance in cancer of the three GTSE1 phosphorylation sites found in the current study using CPTAC data[44]. Color intensity reflects the log2-transformed Z-scores of identified GTSE1 phosphopeptides, indicating relative phosphorylation levels across various tumor cohorts compared to adjacent normal tissues. The complete analysis of all phosphorylation sites can be found in Figure supplement 3D.

Figure 3: GTSE1 protein is stabilized upon its phosphorylation by cyclin D1-CDK4

A) Immunoblot analysis of whole cell extracts from parental HCT-116 cells, AMBRA1 KO HCT-116 cells, and HCT-116 cells expressing either wild-type cyclin D1 or an AMBRA1-insensitive mutant of Cyclin D1 (T286A), in the presence or absence of the CDK4/6 inhibitor palbociclib.

B) Immunoblot analysis of whole cell extracts from HCT-116 cells harboring an endogenous mini-AID domain fused to AMBRA1 N-terminus. Cells were subjected to either incubation with auxin and doxycycline to induce AMBRA1 degradation or transfection with cyclin D1(T286A) in the presence or absence of Palbociclib.

C) Cycloheximide (CHX) chase assay in HCT116 cells with mAID-AMBRA1, treated with or without auxin and doxycycline to induce AMBRA1 degradation. Immunoblot analyses were conducted to assess the stability of GTSE1 and other indicated proteins, with the stable protein SKP1 used as a loading control.

D) Protein stability assessment via CHX chase in U2OS parental cells and AMBRA1 knockout clones (C11 and G11). The protein levels of AMBRA1, GTSE1, and cyclin D1 were analyzed by immunoblotting, with tubulin serving as a loading control.

E) U2OS cells stably transduced with retroviruses expressing the indicated GTSE1 constructs were subjected to cycloheximide CHX chase assays. Subsequent immunoblotting was conducted for the indicated proteins, with tubulin utilized as a loading control.

F) Densitometric quantification of GTSE1 band intensity from (E) and two identical experiments normalized using tubulin. Initial band intensity at time 0 is set as the 100% reference point. Error bars represent SEM (n=3 of biological replicates).

G) Time-lapse microscopy images of U2OS cells stably expressing EGFP-tagged the indicated GTSE1 constructs during a CHX chase. The EGFP signal intensity corresponds to GTSE1 levels, while cells are stained with a far-red cell tracker for cell masking.

H) Quantitative analysis of EGFP fluorescence intensity from time-lapse experiment shown in (G) plus two identical experiments. The initial fluorescence intensity was normalized to 100% at time zero. Data represent the mean fluorescence intensity from the three independent measurements, with error bars indicating SEM.

I) U2OS cells were treated with various inhibitors for 3 hours before harvest: the proteasome inhibitor MG132, the CRL inhibitor MLN4924, and the V-ATPase inhibitor Bafilomycin A1. Immunoblot analysis of the indicated proteins was performed, with tubulin as a loading control. p62 and LC3 serve as autophagy inhibition controls, while p27 is used as control for CRL- and UPS-dependent degradation.

Figure 4: Increased cell proliferation upon cyclin D1-CDK4-mediated phosphorylation and stabilization of GTSE1

A) Bubble plot derived from CPTAC data analysis showing the correlation between the abundance of the bulk phosphopeptides of GTSE1 and the levels of proteins involved in cell proliferation or cell migration across various cancer types. The color intensity of each bubble represents the Spearman correlation coefficient, while the bubble size indicates the negative log10 transformation of the p-values. Bubbles outlined in black indicate statistically significant correlations with q-value < 0.0001, adjusted by Benjamini-Hochberg (BH) method.

B) Growth curve analysis comparing the proliferation of U2OS cells stably expressing GFP-tagged wild-type GTSE1, GTSE1 Tetra SA (phospho-deficient), or GTSE1 Tetra SD (phospho-mimetic). GTSE1 Tetra SD cells proliferated significantly more than cells expressing either wild-type GTSE1 or GTSE1 Tetra SA. Statistical significance was determined using unpaired T-tests with p-values<0.05. Error bars represent the mean +/- SEM (n=3 per condition).

C) Proliferation analysis using CellTrace™ Far Red dye to assess the division of U2OS cells expressing wild-type GTSE1, Tetra SA, and Tetra SD, alongside a comparison between parental and AMBRA KO U2OS cells. Following staining, the dye dilutes progressively with each cell division, allowing for the distinction of successive generations by the relative decrease in fluorescence intensity. Fluorescence-activated cell sorting was employed to accurately measure the dye dilution and thereby quantify the discrete populations representing each generation of the cell line. The gating strategy was implemented to identify live, single cells positive for GFP, as detailed in Figure supplement 4C. The percentages of cells in each generation are as follows: Parental (Undivided: 1.9%, Gen 1: 28.6%, Gen 2: 55.0%, Gen 3: 14.3%, Gen 4: 0.46%), AMBRA KO (Undivided: 1.2%, Gen 1: 5.8%, Gen 2: 28.77%, Gen 3: 54.0%, Gen 4: 10.8%), WT GTSE1 (Undivided: 1.2%, Gen 1: 21.7%, Gen 2: 56.36%, Gen 3: 20.7%, Gen 4: 0%), Tetra SA GTSE1 (Undivided: 5.4%, Gen 1: 37.8%, Gen 2: 55.5%, Gen 3: 0%, Gen 4: 1.2%), and Tetra SD GTSE1 (Undivided: 2.52%, Gen 1: 12.3%, Gen 2: 45.9%, Gen 3: 33.52%, Gen 4: 4.96%). See additional biological replicates in Figure Supplement 4D-E.

Figure Supplement Legends

Figure Supplement 1

A) Schematic of the bioinformatics workflow implemented to identify potential substrates of the D-type cyclins. The process integrates proteomic data from AMBRA1 knockout (KO) U2OS cells versus parental cells[11], protein annotations of the CDK phosphorylation consensus site [S/T*]PX[K/R] from PhosphoSitePlus[24], and cancer-related databases.

B) Kaplan-Meier curves representing the overall survival analysis based on the 50% upper versus lower expression levels of GTSE1. Survival analysis was conducted across the indicated cancer cohorts. The hazard ratio (HR) was calculated to estimate the relative risk, and significance was assessed using the log-rank test with a threshold of $p<0.05$. Curves were generated using the GEPIA2 platform [42].

Figure Supplement 2

A) Phylogenetic Conservation of GTSE1 Phosphorylation Sites Across Species. Illustration of the evolutionary conservation of phosphorylation sites within the GTSE1 protein.

B) The sequence alignment highlights identical (red) and similar residues (orange) across a range of species, indicating the conserved nature of these phosphorylation sites in GTSE1 orthologs.

Figure Supplement 3

A) HEK293T cells transfected with the indicated single Ser-to-Ala mutants of HA-tagged GTSE1, with and without Cyclin D1-CDK4 co-expression, followed by analysis of their migration pattern on phos-tag™ gels.

B) Immunoblot analysis displaying cell cycle synchronization effects following 72 hrs of serum starvation in parental T98G cells and AMBRA1 KO T98G cells. Cells were collected at various time points post-serum re-supplementation as indicated, followed by immunoblotting with the indicated antibodies. Cyclin A2 and Cyclin B1 serve as S phase and G2-M markers, respectively. pH3 at Ser10 serves as a mitotic marker. GAPDH serves a loading control.

C) Heatmap illustrating differential abundance of GTSE1 phosphorylation in cancer using CPTAC data[44]. Color intensity reflects the log2-transformed Z-scores of identified GTSE1 phosphopeptides, indicating relative phosphorylation levels across various tumor cohorts compared to adjacent normal tissues.

D) HEK293T cells were subjected to transfection with the indicated variants of HA-tagged GTSE1, with and without FFSS-Cyclin D1-CDK4 co-expression. Where indicated, cells were treated with Palbociclib for 4 hrs before harvest. Finally, samples were subjected to western blot analysis with the indicated antibodies.

E) HCT mAID FLAG-AMBRA KI cells underwent pull-down using an anti-FLAG antibody versus an IgG sham pull-down. Where indicated, cells were treated with MLN4924 for 3 hours prior to harvesting. Western blot analysis was performed using the specified antibodies to compare the pull-down fraction with the whole cell extract (WCE). Vinculin serves as WCE loading control.

Figure Supplement 4

A) Bubble plot derived from CPTAC data depicting the correlation GTSE1 protein abundance with the levels of proteins involved in cell proliferation or cell migration across various cancer types. Data analysis was performed as detailed in Figure 4A.

B) Growth curves comparing the proliferation of AMBRA1 KO clones with that of parental U2OS cells, with graphs displaying mean cell counts at each time point, n=3 biological replicates per clone. Statistical significance was determined using unpaired T-tests with p-values<0.05. Error bars represent SEM.

C) Gating strategy for FACS analysis shown in Figure 4C. The gating strategy was implemented to identify live, single cells positive for GFP. The fourth panel (proliferation analysis) is the same as the first panel in Figure 4C (GTSE1), which is used here to show the gating strategy.

D-E) Independent biological replicates of cell proliferation analysis using CellTrace™ as shown in Figure 4C. Generation distribution in D: WT GTSE1 (Undivided: 2.6%, Gen 1: 8.5%, Gen 2: 44.0%, Gen 3: 39.7%, Gen 4: 5.4%), Tetra SA GTSE1 (Undivided: 0.1%, Gen 1: 5.5%, Gen 2: 44.5%, Gen 3: 50.0%, Gen 4: 0%), and Tetra SD GTSE1 (Undivided: 1.0%, Gen 1: 4.5%, Gen 2: 40.0%, Gen 3: 34.4%, Gen 4: 20.0%).Generation distribution in E: WT GTSE1 (Undivided: 16.8%, Gen 1: 52.9%, Gen 2: 27.9%, Gen 3: 2.5%, Gen 4: 0.3%), Tetra SA GTSE1 (Undivided: 22.0%, Gen 1: 49.7%, Gen 2: 24.8%, Gen 3: 3.3%, Gen 4: 0%), and Tetra SD GTSE1 (Undivided: 10.0%, Gen 1: 38.0%, Gen 2: 40.0%, Gen 3: 10.1%, Gen 4: 1.5%).

F) Representative cell cycle analysis of U2OS cells expressing wild-type (WT), Tetra SA, and Tetra SD constructs. Cells were pulsed with EdU and stained with propidium iodide (PI) for DNA content assessment. Cell cycle distribution was quantified by FACS using the gating strategy described in panel C. Graph on the right shows the percentage of cells in each phase of the cell cycle: AMBRA Parental (G1: 42.9%, S: 46.2%, G2/M: 10.8%), AMBRA KO (G1: 35.0%, S: 51.7%, G2/M: 13.0%), WT GTSE1 (G1: 45.0%, S: 43.8%, G2/M: 11.2%), Tetra SA GTSE1 (G1: 45.4%, S: 42.2%, G2/M: 11.8%), and Tetra SD GTSE1 (G1: 38.6%, S: 46.6%, G2/M: 14.0%).

A

GENE	Log2FC	adjp
CCND1	6.7140	4.138e-10
APLP2	5.8330	5.745e-05
DIAPH3	5.5340	7.336e-04
DGKA	5.2600	3.799e-03
CCND3	5.0440	1.017e-02
PNISR	5.0440	1.017e-02
SDE2	5.0440	1.017e-02
APBB1	4.9230	1.607e-02
ARAP3	4.7900	2.855e-02
RAB11A	4.0850	2.880e-02
CCND2	3.5990	7.434e-15
PLK1	3.3600	1.675e-03
DDX19A	3.1030	4.370e-03
CDK4	3.0740	9.300e-13
AURKB	2.7290	1.233e-02
SP1	2.5450	3.598e-03
GTSE1	2.4310	2.030e-03
CDKN1A	1.9250	8.827e-03
PRAME	1.8090	7.336e-04
CDKN1B	1.6590	1.192e-02
NFKB1	1.3930	1.233e-02
TOP2A	0.8265	5.740e-12
DNMT1	0.7194	3.598e-03
KIF2C	0.7005	1.009e-02
MKI67	0.6980	1.014e-05
KRT17	-0.5590	9.669e-04
DPYSL3	-0.5929	3.401e-02
AHNAK2	-0.6921	1.861e-02
MAP1A	-0.8703	2.880e-02
PPP1CB	-1.4580	3.401e-02

B

GENE	MOD_RSD	SITE_+/-7_AA	Log2FC
PNISR	S611-p	RERRRNRsPsRERRR	5.0440
ARAP3	S695-p	VSNKAGPsPPRRGRD	4.7900
GTSE1	S262-p	PKKEIPAsPsRTKIP	2.4310
CDKN1A	S91-p	TCTLLPHsPERPEAS	1.9250
CDKN1B	S183-p	DGsPNAGsVEQtPKK	1.6590
NFKB1	S892-p	IEVIQAAssPVKtTs	1.3930
TOP2A	S1351-p	DDEDFVPsDAsPPKT	0.8265
DNMT1	S127-p	VGMADANsPPKPLsk	0.7194
KIF2C	K534-ub	IRALGQNkAHtPFRE	0.7005
MKI67	S325-p	GKGRDVEsVQtPskA	0.6980
DPYSL3	S518-p	kGGtPAGsArGsPtR	-0.5929
AHNAK2	T228-p	VADGCREtPTKTLEG	-0.6921
MAP1A	S1200-p	DTQsLsLsEEsPSKE	-0.8703
PPP1CB	T316-p	LNsGRPVtPPRTANP	-1.4580
PRKD2	T619-p	NLECMFEtPEKVFVV	-4.7900

C

GENE	Log2FC	Log2FC_ctr	adjp_ctr	Log2FC_ambra	adjp_ambra
GTSE1	2.4310	-4.084	1.098e-01	-6.521	5.571e-09
TOP2A	0.8265	-2.677	6.013e-47	-2.044	2.496e-14
DNMT1	0.7194	-1.355	5.816e-07	-1.379	1.651e-10
KIF2C	0.7005	-2.368	2.730e-13	-2.542	3.325e-24
MKI67	0.6980	-3.475	1.772e-52	-2.611	3.218e-43

D

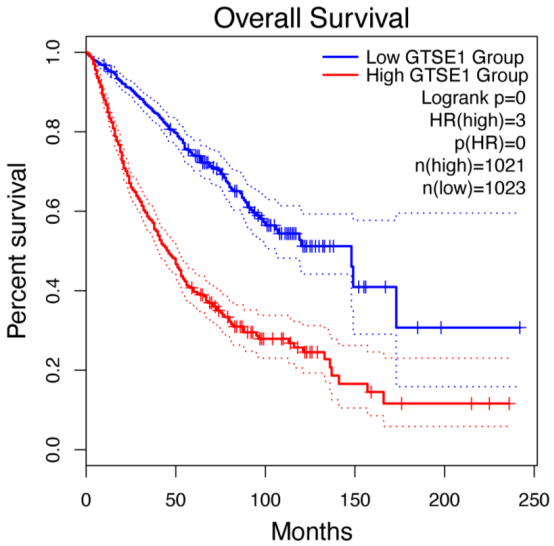

E

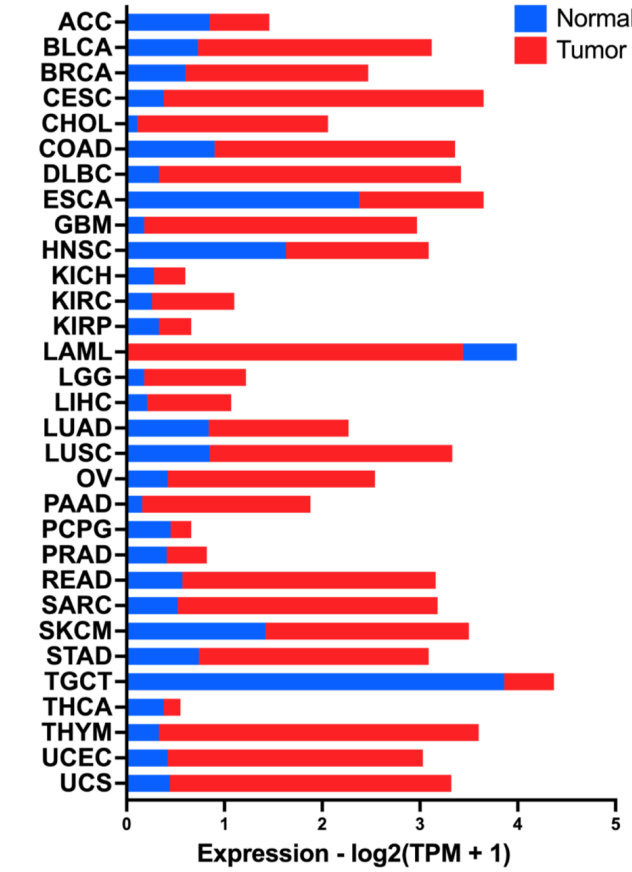

F

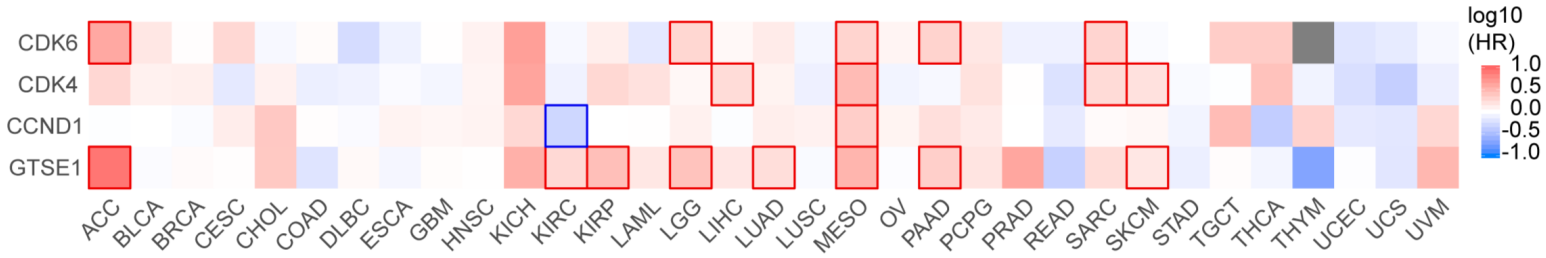

Figure 1 - García-Vázquez et al.

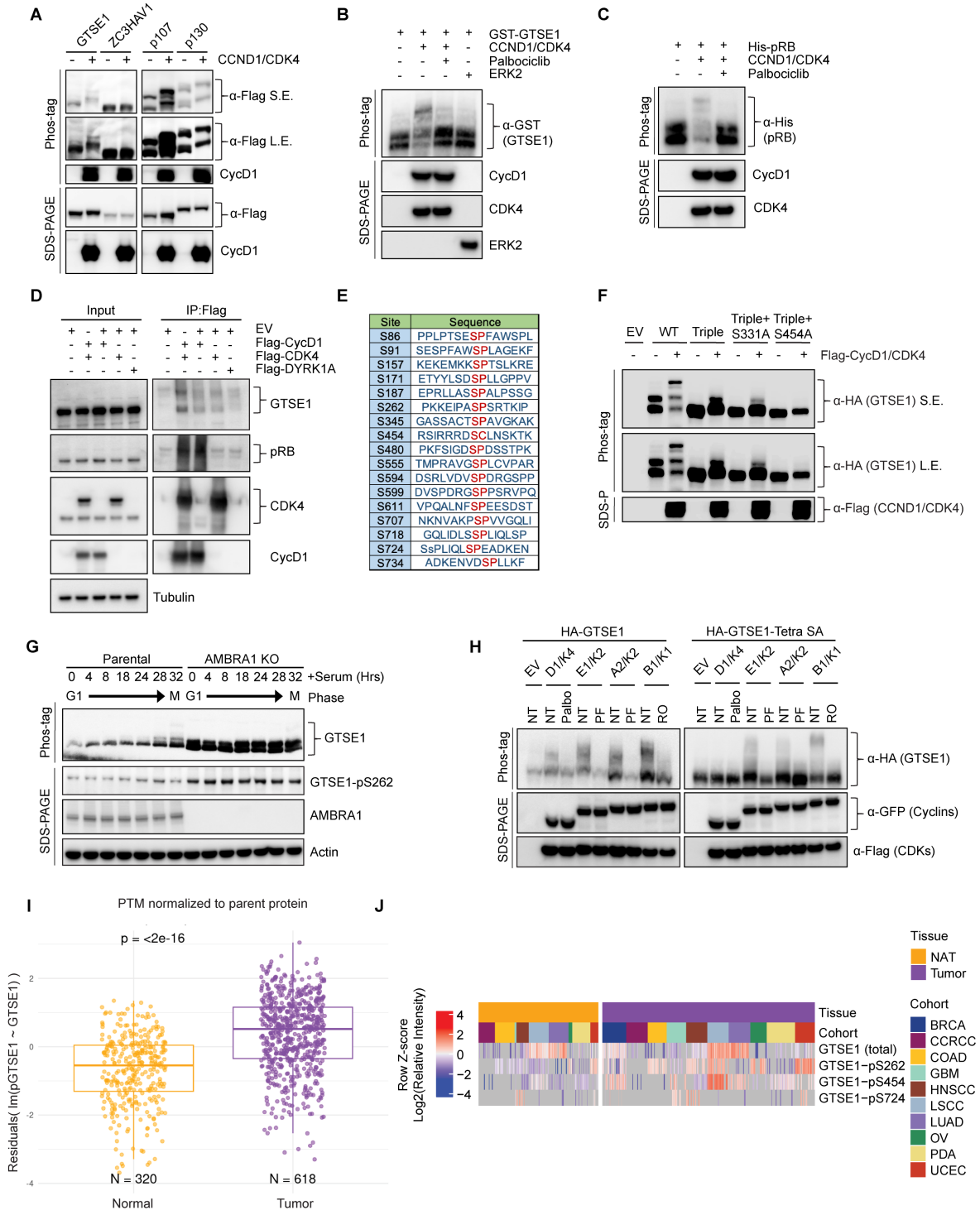

Figure 2 - García-Vázquez et al.

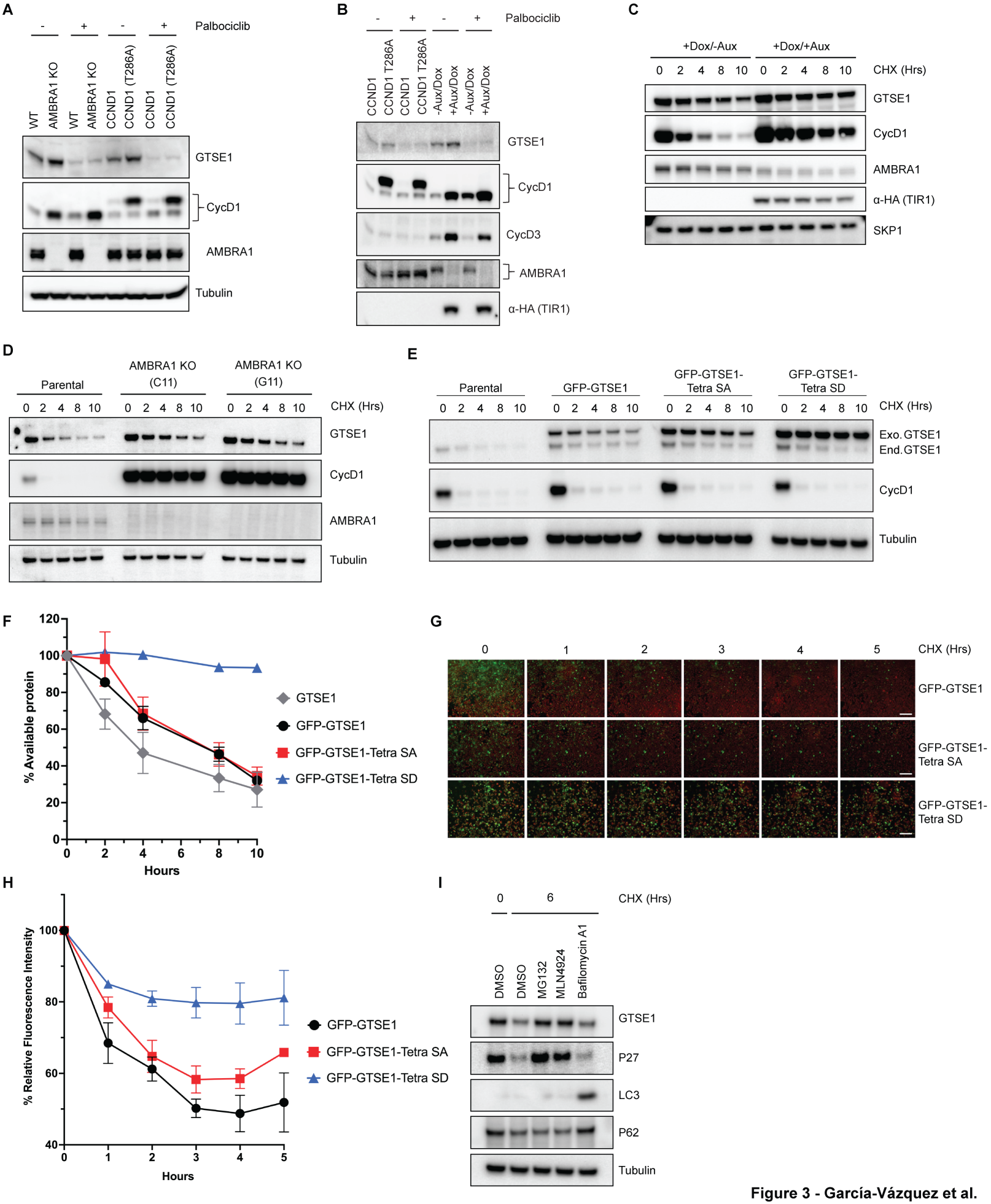

Figure 3 - García-Vázquez et al.

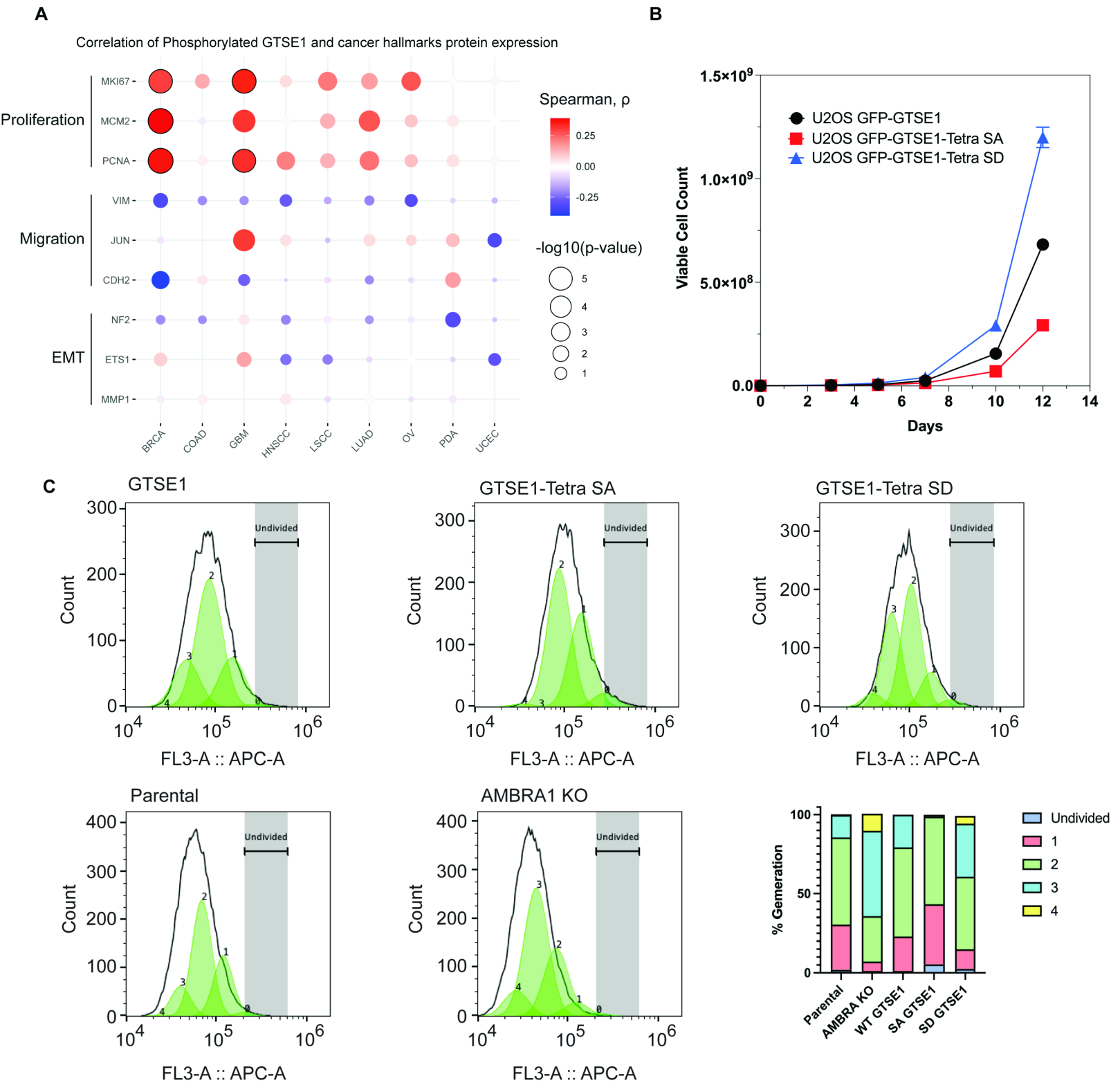

Figure 4 - García-Vázquez et al.

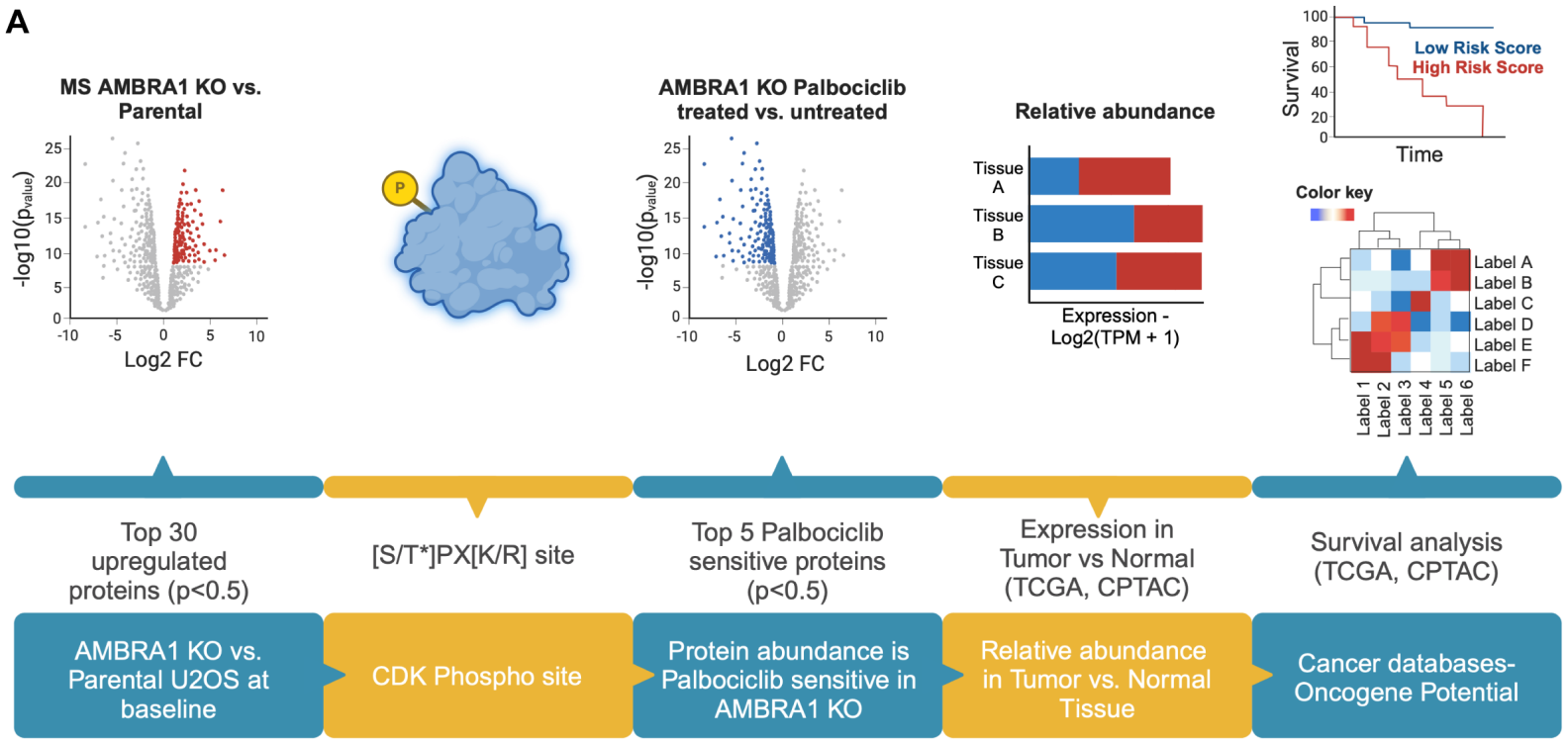

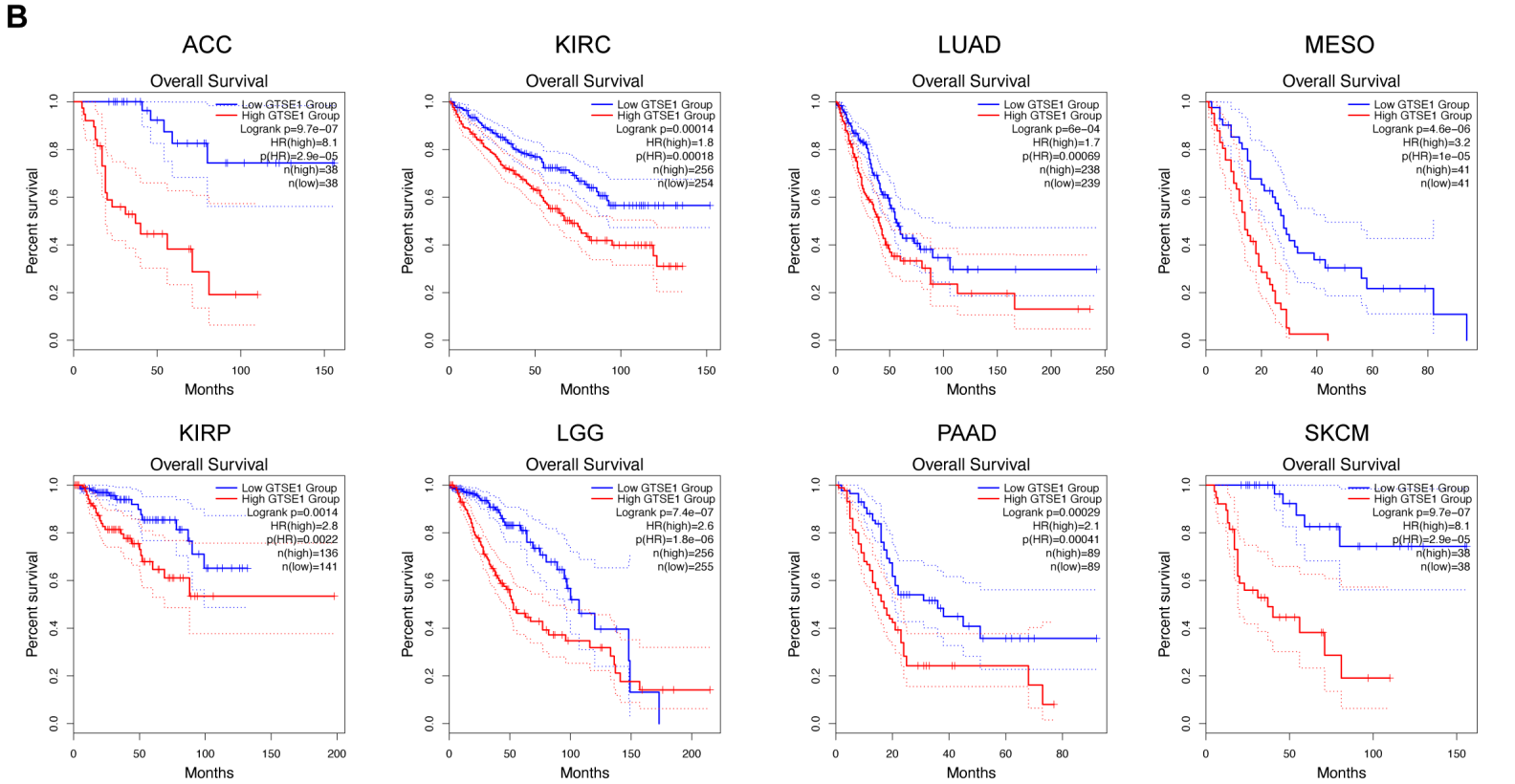

Figure Supplement 1 - García-Vázquez et al.

A

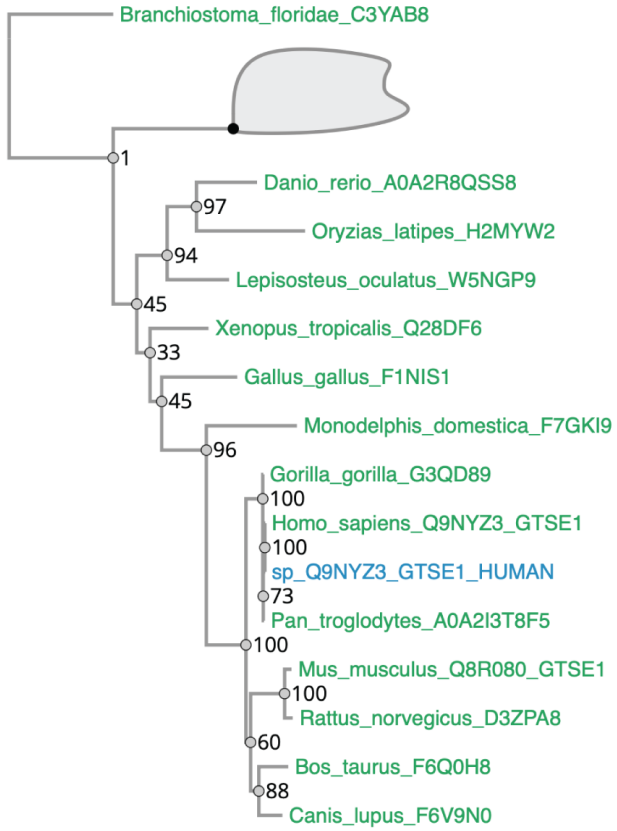

B

Site	Species	Sequence
S86	Homo sapiens	PPLPTSESPFAWSPL
	Rattus norvegicus	PLAPGSGSPCTWSPL
	Mus musculus	PLAPGSGSPCTLSPL
	Gallus gallus	KRVPISDEKLTWSPL
	Branchiostoma floridae	-----EEEKFVPLEL
S91	Homo sapiens	SESPFAWSPLAGEKF
	Rattus norvegicus	SGSPCTWSPLTGEKF
	Mus musculus	SGSPCTLSPLTGEKF
	Gallus gallus	SDEKLTWSPLTGDKF
	Branchiostoma floridae	EEEKFVPLELNGDQY
S157	Homo sapiens	KEKEMKKSPTSLKRE
	Rattus norvegicus	EQKRDKSPLSLKRE
	Mus musculus	KEQKRDRSPMSLKRE
	Gallus gallus	HH-IEKSPRAVKRE
	Branchiostoma floridae	KAPQNSPRNSPRRM
S171	Homo sapiens	ETYYLSDSP--LLGPPV
	Rattus norvegicus	ETFCLPSS---RAQPLL
	Mus musculus	ETFCLPSS---RV-QPPM
	Gallus gallus	ETFCVGDSPacMLLPSFQ
	Branchiostoma floridae	MTYTLDT[5]ASssTTTADVQ
S187	Homo sapiens	EPRLLASSPAL--PSSG
	Rattus norvegicus	EPQLLA-SPGLPNS-
	Mus musculus	EPQLLA-SPGLLSS-
	Gallus gallus	KESDKL----LPGDK
	Branchiostoma floridae	DSTQRQeNNEVKEGQ
S262	Homo sapiens	PKKEIPASPSRTKIP
	Rattus norvegicus	LKKEVPASLQQTKPL
	Mus musculus	LKKEVPASIQRTKLV
	Gallus gallus	AKPGRQTNISTKRDS
	Branchiostoma floridae	IKPGI-------RK[16]A
S345	Homo sapiens	GASSACTSPAVGKAK
	Rattus norvegicus	LVSGVGRSPTAGKAK
	Mus musculus	LESGVYRSSVAGKAK
	Gallus gallus	SVSSNLNSSL[4]IGKNG
	Branchiostoma floridae	TNPSQGSLGR[3]NGSID
S454	Homo sapiens	RSIRRRDSCLNSKTK
	Rattus norvegicus	VSIKRQDSSLGCKTE
	Mus musculus	VSIKRRDSYLSCKTE
	Gallus gallus	GSTTKGSLCPKPRAR
	Branchiostoma floridae	AASANTSFSKKSLLP
S480	Homo sapiens	PKFSIGDSPDSSTPK
	Rattus norvegicus	PQFSVGESPDRVTPK
	Mus musculus	PQFSVGESPGGVTPK
	Gallus gallus	PVKAGDITPNKSATK
	Branchiostoma floridae	PMRATLPMSQISTPK
S555	Homo sapiens	TMPRAVGSPLCVPAR
	Rattus norvegicus	SMPRALVSPLCVPAR
	Mus musculus	SMPRALVSPLCVPAR
	Gallus gallus	TTPRTVFSPRIESVR
	Branchiostoma floridae	SSRRRSGIPTPRSMQ
S594	Homo sapiens	DSRLVDVSPDRGSPP
	Rattus norvegicus	GQSQGLSSDESSSPP
	Mus musculus	GQAQGLSSDESSSPP
	Gallus gallus	------SSEDDPSPP
	Branchiostoma floridae	SCLPTLAANDSPSEF
S599	Homo sapiens	DVSPDRGSPPSRVPQ
	Rattus norvegicus	LSSDESSSPPSSVPQ
	Mus musculus	LSSDESSSPPSSVPQ
	Gallus gallus	*-SSEDDPSPPPVLPL
	Branchiostoma floridae	LAANDSPSEFPATHL
S611	Homo sapiens	VPQALNFSPEESDST
	Rattus norvegicus	VPQALNFSPEKSDFP
	Mus musculus	VPQALNFSPEKSASP
	Gallus gallus	LPLMLDFSPEKAVI-
	Branchiostoma floridae	THLR----------
S707	Homo sapiens	NK-NVAKPSPV-VGQLI
	Rattus norvegicus	GRSDVGKPPKAELGQLI
	Mus musculus	GRNDVGKPAKAELGQLI
	Gallus gallus	NKVIPLKPVFSEQIKLI
	Branchiostoma floridae	----------
S718	Homo sapiens	GQLIDLSSPLIQLSP
	Rattus norvegicus	GQLIDLGSPLIQLSP
	Mus musculus	GQLIDLGSPLIQLSP
	Gallus gallus	IKLIDLSSPLITLSP
	Branchiostoma floridae	-------KPLIDFGE
S724	Homo sapiens	SSPLIQLSPEADKEN
	Rattus norvegicus	GSPLIQLSPEADKEN
	Mus musculus	GSPLIQLSPEADKEN
	Gallus gallus	SSPLITLSPDINKEN
	Branchiostoma floridae	-KPLIDFGEEDMKTN
S734	Homo sapiens	ADKENVDSPLLKF
	Rattus norvegicus	ADKENVDSPLLKF
	Mus musculus	ADKENVDSPLLKF
	Gallus gallus	INKENLDSPLLKF
	Branchiostoma floridae	DMKTN--SPAIAN

Figure Supplement 2 - García-Vázquez et al.

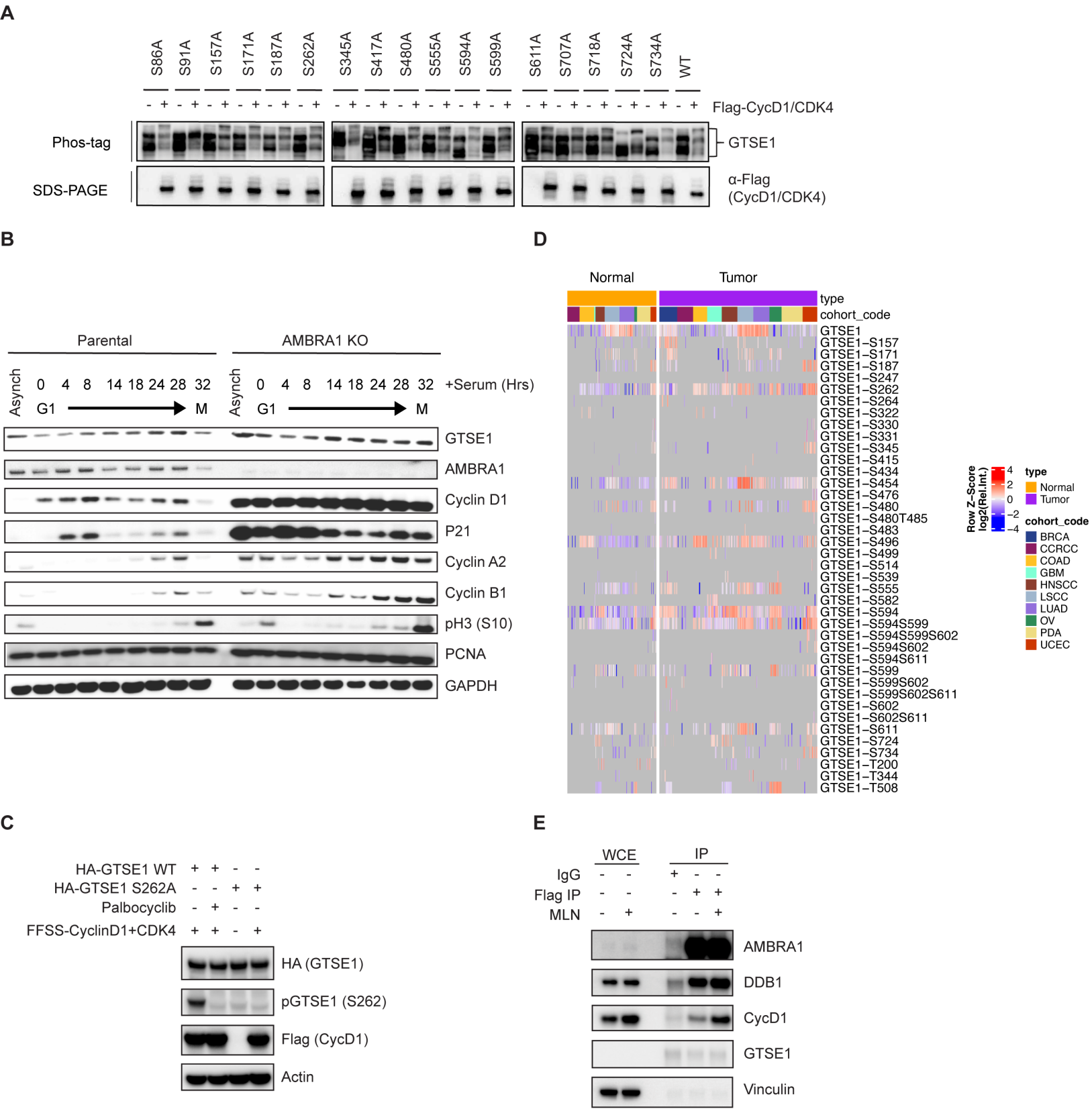

Figure Supplement 3 - García-Vázquez et al.

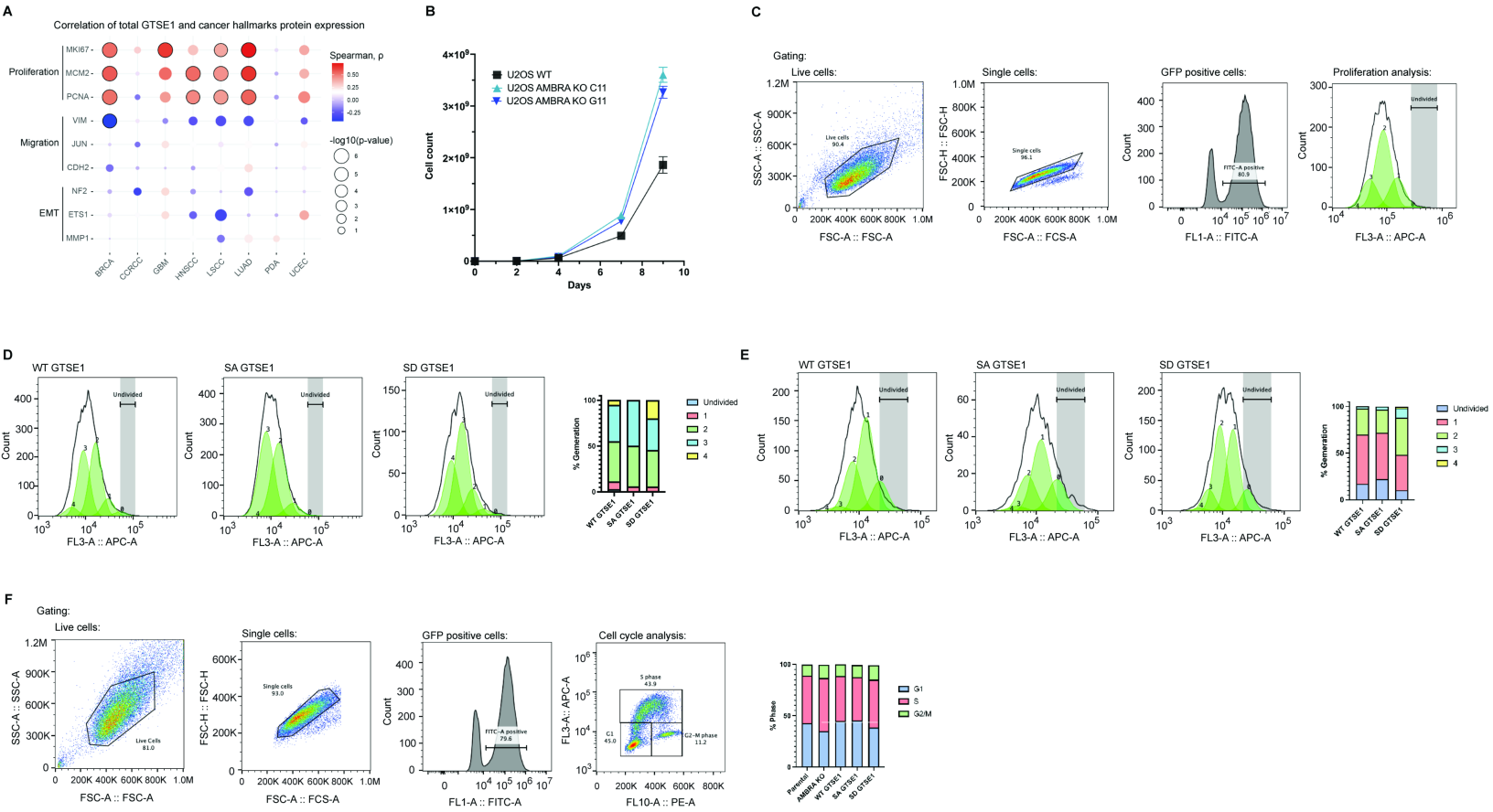

Figure Supplement 4 - García-Vázquez et al.